*Article*

# Exploring Reduced Graphene Oxide Sheets Stabilized by Cu(II) and Cu(I) Cations in Ethanol

Aya Jezzini [1,2], Anne Davidson [1], Tayssir Hamieh [2,3,*] and Joumana Toufaily [2]

[1] Laboratoire de Réactivité de Surface LRS, UMR 7197, Sorbonne Université, 75005 Paris, France; jizziniaya@hotmail.com (A.J.); anne.davidson@sorbonne-universite.fr (A.D.)

[2] Laboratory of Materials, Catalysis, Environment and Analytical Methods (MCEMA), LEADDER, Faculty of Sciences, Lebanese University, Hadath P.O. Box 6573, Lebanon; joumana.toufaily@ul.edu.lb

[3] Faculty of Science and Engineering, Maastricht University, P.O. Box 616, 6200 MD Maastricht, The Netherlands

* Correspondence: t.hamieh@maastrichtuniversity.nl

**Abstract:** In this study, ultrasound treatment was used to exfoliate commercially available graphite flakes into reduced graphene oxide (rGO) dispersed in ethanol. After centrifugation, solid copper chloride trihydrate was added, resulting in a green liquor containing Cu(II), Cu(I), and rGO. These liquors exhibited good and rapid photocatalytic activity in the degradation of eosin and bromophenol blue dyes (elimination in a few seconds) under visible-light irradiation. UV–visible spectroscopy confirmed the presence of rGO and Cu species. The size and morphology of the rGO sheets were investigated by several methods (SAXS, wide-angle XRD, SEM, and TEM). Negative UV peaks indicated light emission, which was independently verified by fluorescence. Intense plasmon peaks, with absorbances greater than 10, were observed after adding copper chloride salt. These plasmons were eliminated by a high dilution before the described catalytic tests were performed.

**Keywords:** photocatalysis; $Cu^{2+}$ and $Cu^+$; graphite; ultrasound; plasmons; dye decomposition

## 1. Introduction

A single or a few layers of 2D graphene sheets have excellent mechanical and optical properties. They comprise carbon atoms arranged to form a honeycomb structure, defined by carbon atoms in a $sp^2$ hybridization, as described in a general public magazine in 2008 [1]. The word graphene begins with graph—to recall the carbon species. Its ene end is associated with its polycyclic aromatic hydrocarbon nature [2]. The electrons inside the sigma bonds and between the carbon atoms are stable. Its extraordinary optical properties are a result of the electrons inside the atomic $2p_z$ orbitals of the carbon atoms. These atomic orbitals overlap and extended valence bonding $\pi$ and conducting anti-bounding $\pi^*$ molecular orbitals are formed. Intraband and interband electronic transitions in the spectral ranges of UV, visible, and far infrared are observed.

The introduction of graphene in photocatalysis was reviewed in 2016 [3]. Several methods have been developed, used, and discussed in the literature to achieve the exfoliation of graphite. Current exfoliation methods and techniques used to produce single-layer materials from graphite precursors were described by Minzhen et al. [4]. The UV–visible NIR absorption spectra of reduced graphene particles are complex, mainly because of electron interactions. The first detailed general description of electron interactions was published recently by Maier [5]. Transition metal ions can be coordinated on a reduced graphene surface [6–8]. With added copper chloride, reduced graphene oxide (rGO) particles, called plasmons, exhibit strong absorption [9]. If graphene particles are suspended in a solvent, they will have indirect semi-conducting properties, and a band-gap can be detected between their valence and conduction bands [10,11]. These bands' positions in energy are influenced by the graphene nanoparticles' sizes, shapes, and defects (O-containing and structural). This study addresses four questions:

1. Is the added copper chloride hydrated salt necessary to observe plasmons?
2. Can plasmon positions and intensities be adjusted by dilution?
3. Can plasmon coupling with C-C vibrations be evidenced?
4. Can plasmons be eliminated to study photocatalytic properties attributed to copper species and reduced graphene particles?

These questions are addressed using UV-visible–NIR spectra. Small negative peaks in the UV range suggest fluorescence, and this was independently verified for the graphene sheets before the addition of copper. Diluted and special cells (0.2 cm instead of 1 cm optical path) were compared to suppress plasmons. When suppressed, band-gap measurements of the C species were conducted using classical and new methods [10–15]. Optical characterizations and band-gap values were compared with published data [16,17]. Catalytic tests for eosin and bromophenol blue dye decomposition, under visible-light irradiation over copper/graphene, are also introduced.

Several authors have described nanoscrolls and their potential uses [18–21]. We have reported that ultrasound techniques can be used to exfoliate them, and 3D graphite GR particles can be used to obtain flat particles for use as supports for Zn–ferrite nanoparticles to eliminate antibiotic traces of the antibiotic amoxycillin [15]. In the most common preparation method using ultrasound in water, graphene oxide (GO) sheets are obtained using the Hummers method. GO is then reduced to give rGO, and three distinct reducers are used: hydrazine, ascorbic acid, and natural extracts of Amaranthus hybrids [18]. Here, ethanol was used as solvent and also as a reducer [15]. Some of the reported data concern samples prepared using ultrasound indirectly in thermostatic beakers, samples introduced in a water bath, or a horn introduced inside the solution that can be water [19], ethanol [20], or water with strong mineral acids. Solid catalysts containing doped oxide nanoparticles dispersed on porous nanocrystals of zeolite FAU or rGO, for instance, are interesting in oxidation reactions of oxygen and also in the degradation of pollutants [22–32]. They have also been used for biomedical applications [29]. The catalysts Cu/Zn on graphene have been formed by CVD [33]. To avoid graphene agglomeration, neutral surfactants and negatively charged species can be added. But a simple addition of organics affects the physical and chemical properties of graphene sheets. Here, similar solids are obtained by using a simple contact of suspended graphene nanoparticles with the mineral species $CuCl_2 \cdot 3H_2O$ after an ultrasound treatment aimed at eliminating the nanoscrolls of graphene and a centrifugation to remove graphite 3D particles. Solids characterizations are performed by XRD, SEM, and TEM micrographs, associated with selected area electron diffraction. We will focus on the description of the plasmon intensities and positions as a function of the Cu/rGO dilution in ethanol.

## 2. Materials and Methods

### 2.1. Materials

Commercial, natural graphite flakes, GR, 99% carbon, 100 mesh, were sourced from Sigma Aldrich n° 808091, CAS 7782-42-5, Paris, France; they were polluted in carbon nanoscrolls similar to the ones described by several authors [18–21]. We used absolute alcohol, CAS 64-17-5, and $CuCl_2 \cdot 3H_2O$, CAS 10125-13-0, from the same company. All these reagents lacked intrinsic toxicity. Here, we focused on working with the catalysts in a liquid state and on their dilution in ethanol. The graphene suspensions contained reduced graphene rGO, and they were easily recognized because of their black color. Ultrasound treatment was applied directly inside the centrifugation vials to warrant the absence of unwanted contamination by metallic species and to ascertain that the containers always had the same shape and volume. The vials had a basic conical shape and a height of 115 cm. They contained between 40 and 45 mL of ethanol. The effect of dispersion by organic solvents such as N-methyl-pyrrolidone was described by Politano and Chiarello [34]. The aromatic molecules were replaced by ethanol and an inorganic copper salt because they can alter the electronic properties of rGO.

## 2.2. Methods

Scanning electron microscopy (SEM) imaging was performed with a Hitachi SU-70 FESEM (Hitachi, Paris, France). Transmission electron micrographs were registered on a JEOL JEM 2011 UHR (Jeol, Croissy-sur-Seine, France) microscope, operating at 200 kV, and equipped with an ORIUS Gatan Camera (Paris, France). For the observations, the liquids were deposited on 3 mm copper grids coated with an amorphous carbon film and let dry.

Ultrasonic irradiations were generated by a Vibracell VCX 500 apparatus (Bioblock, Paris, France) (500 W power, used at 40%, with a frequency of 20 kHz). The horn of this apparatus, 13 mm in diameter, was made with an alloy of Ti-6Al-4V and warranted for an overall volume of solution of 50 mL. The probe penetrated 6 cm inside the used liquid inside the vial. We used constant irradiations for 5, 6, or 7 min or for 2 h with and without pulses of 15 s and stops of 15 s. Experimental conditions, the influence of the ultrasound power, several sonication times, and the initial graphite concentration were detailed by Navik et al. [23]. The used initial concentration of graphite was equal to 5 mg/mL. The sonication was realized in a sonication bath with a power of 1.08 kW. In a previous study [23], Navik et al. were interested in graphene stabilization by an organic molecule, curcumin, stable for a graphene concentration of 1.44 mg/mL; their study also contained complementary data concerning the detection of graphene sheets in ethanol with several initial GR concentrations. There is one main difference between these published results and ours: the used ultrasound horn penetrates deeply into the solution. In our liquors, to avoid solids precipitation, we used 6 min or 2 h of ultrasound treatment, and the initial graphite was introduced in concentrations lower than 0.5 mg/mL. After the ultrasonic treatment, a centrifugation was applied at 3000 and/or 5000 rotations by min, rpm, and 12 min. Bulk 3D graphite was recovered at the bottom of the flask. Its 3D character was demonstrated by SAXS measurements (Figure S1), and it was eliminated. The transparent black liquor was then used directly to dissolve the salt, copper chloride trihydrate. The solution was changing color spontaneously and became green in less than 2 min. We were surprised to observe that the green color of the solution was extremely stable, remaining constant even after several months of storage in air, whereas the species that we have detected that can be green are Cu(I) cations, and are known to be instable; therefore, only the redox potential of the couple Cu(II) Cu (metal) is given in the literature. To explain their stability, a positive role of ethanol to protect them is proposed.

The presence of the graphene sheets in suspension in ethanol was studied first by WAXS wide-angle Scattering on a Bruker-type D8 Advance (Paris, France) within the range of $2\theta$ from $0.3°$ to $90°$ with copper 1.54186 Å, a mixture of K$\alpha_1$ and K$\alpha_2$, and a ratio of 1 for 2. A Bragg–Brentano set-up was used to obtain graphics in intensities versus $2\theta$. Simulations were created using the Fullprof program. With this program, precise values of peak positions and intensities (integrated units) were obtained. Within the range of 23–31°, three observed peaks were labelled (1), (2), and (3). Peak (1) is a small peak on the left part. Peaks (2) and (3) are more than 5 times more intense and are on the right part. Two additional peaks attributed to X-ray diffusion are presented in Figure 1 to take into account the shape of the diffraction. Peaks (2) and (3) were calculated based on the following parameters: H = FWHM, the Full-Width at Half Maximum, ETA, $\eta$, a linear combination of a Lorentzian $L$, and a Gaussian $G$ line shape with the same FWHM. Expression 1 can be written for XRD:

$$I(2\theta) = I_{hkl}[\eta\, L(2\theta - 2\theta_0) + (1 - \eta)G(2\theta - 2\theta_0)] \tag{1}$$

The Gaussian peak is given by Equation (2):

$$G(2\theta) = C_1 exp[-\pi(2\theta - 2\theta_0)^2/\beta^2] \tag{2}$$

where $C_1$ is the peak intensity, $2\theta_0$ is the $2\theta$ position of the peak maximum, and the integral breadth, $\beta$, is related to the FWHM peak width.
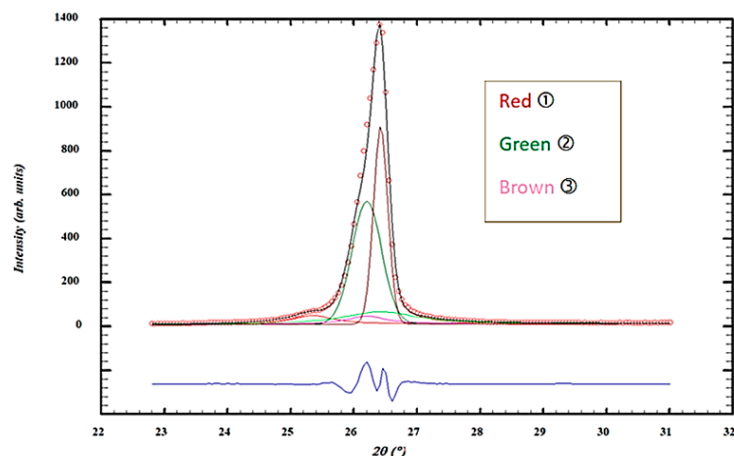
**Figure 1.** Commercial sample, GR. Possible decomposition of an XRD peak into five components: ①, ②, and ③ peaks. Both intense ② and ③ peaks are Gaussian in shape. I (observed) in black with red spots, I (calculated) for three peaks labelled (1) in red, (2) in green, and (3) in brown, and in blue is the difference between I (observed) and I (calculated).

A value of $\eta$ close to zero indicates a Gaussian line shape. Intermediate values between 0 and 1 indicated a pseudo-Voigt shape with given % of *G* and *L*. Two very small diffraction peaks associated with X-ray diffusion are located at the same positions as peaks (2) and (3) and are labelled peaks (4) and (5).

UV–visible–NIR spectra were measured on a Varian 4000 spectrometer (Bimedics, Paris, France) within the range of 200–1400 nm. They were measured in the UV (200 to 400 nm), the visible (400 to 800 nm), and the NIR ranges inside two kinds of quartz cells, one with an optical path of 1 cm and a second with an optical path (internal) of 2 mm. Fluorescence measurements were carried out with a Horiba Jobin Yvon spectrometer Fluorolog®FL3-22 (Horiba, Paris, France). We tried two kinds of florescence measurements, the first one with diluted solutions in ethanol and the second one directly with the concentrated initial solutions obtained by applying ultrasound treatment for 6 min and without centrifugation.

Better results in fluorescence were obtained on the non-diluted solutions and for an angle between the excitation light and detector set at 90° to avoid detector saturation.

## 3. Results

### 3.1. Solid Graphite XRD to Study Mixture of Nanoscrolls and 3D Graphite

In XRD, enlargements between 23 and 31° were performed and analyzed with the program Fullprof. The positions of peaks (2) and (3), labels indicated in the experimental section, are equal to 26.208 and 26.427°, with respective FWHM values of 0.495 and 0.179°; their ETA values are both equal to zero. The two peaks are therefore Gaussian in shape. Peak (3) is the narrowest and can be assigned to 3D graphite (Figure 1).

Particles sizes can be estimated using the Scherer equation in the following form:

$$L_{hkl} = \frac{0.9\,\lambda}{\text{FWHM}_{hkl}\,\cos\theta}, \tag{3}$$

where FWHM = β is expressed in radians. Average particles sizes of 700 and 300 Å are obtained on peaks (2) and (3). These dimensions are too large for nanoparticles (Figure 1).

Peak (2) is attributed to graphene sheets, their varied sizes being associated with a large FWHM of this peak, significantly larger than the one of peak (3), attributed to graphite 3D particles. It is interesting to know that this decomposition of the X-ray diffraction peak is no longer detected when the GR commercial sample is submitted to an ultrasound treatment after its suspension in ethanol for 2 h. In that case, a single XRD peak at 26.54° with a Gaussian shape, which corresponds to the 002 diffraction of reconstructed 3D graphite domains, is observed.

The integrated intensities of peaks (1), (2), and (3) indicate that the percentage of 3D graphite is 60.52% and that of graphene stabilized in nanoscrolls is 36.33%.

*3.2. Observations Correlated to Graphene Particle Sizes*

3.2.1. Measurements Performed on SEM and TEM Images

The SEM image in Figure 2 is relative to graphene nanoscrolls. These nanoscrolls are decomposed after a simple manual grinding. Their diameter, as measured on adjacent nanoscrolls, is 235 nm. A correct evaluation of the two solids is difficult on SEM images only because only a given part of the sample is visible. But relative percentages of the two phases can be obtained using the XRD measurements.
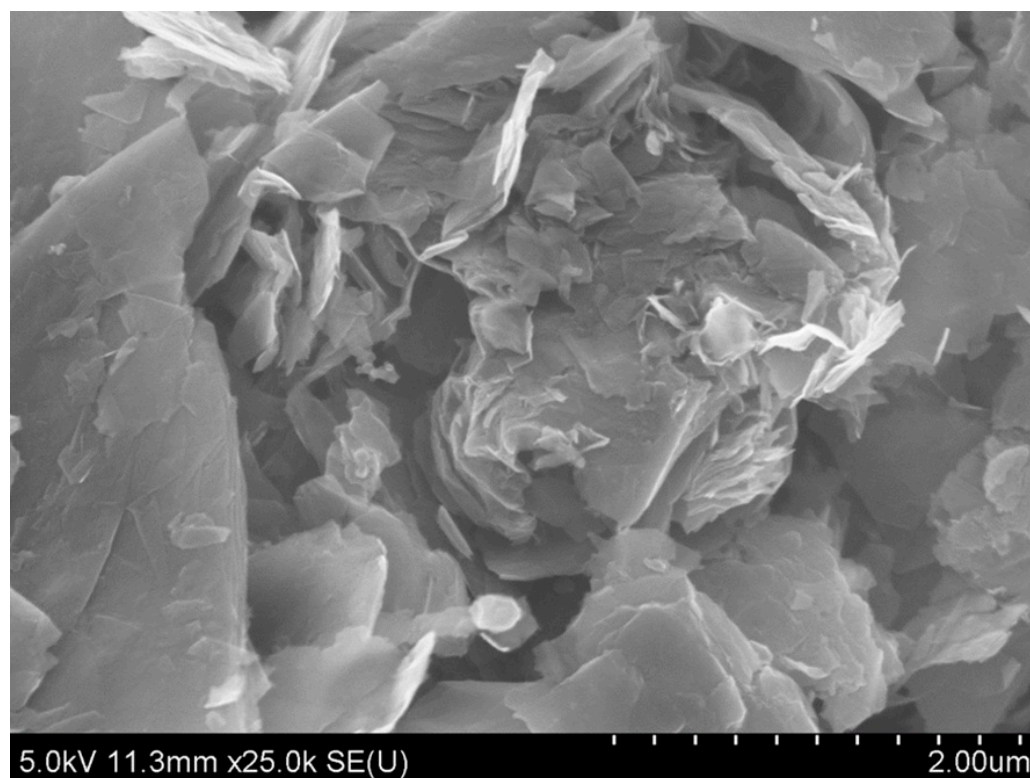


**Figure 2.** SEM images of the nanoscrolls: other images already published [8]. Upper detector used for secondary electron detection. Magnification: ×25,000; scale bar: 2 μm.

After an ultrasound treatment of 6 min with pulses of 15 s and stops of 15 s, the nanoscrolls are no longer detected neither by microscopy nor by XRD. The fact that nanoscrolls can be transformed in flat domains was already known, with bubbles of cavitation being inserted within the main part of the scrolls and destroying them [6]. The present work complements previous studies by showing that the size of the flat nanoparticles is directly affected by the time of the applied ultrasound. Micrometer-sized particles observed after 6 min of ultrasound and drying are replaced by smaller particles of size lower than 100 nm after an ultrasound treatment of 2 h. An additional selected electron diffraction is presented in Figure 3 and was carried out on a graphene particle. This image is important, as it establishes that the studied specific sheet contains five distinct layers. The white spots are indeed grouped in thirds on the Bragg rings, but the medium spot is larger than the two other ones.
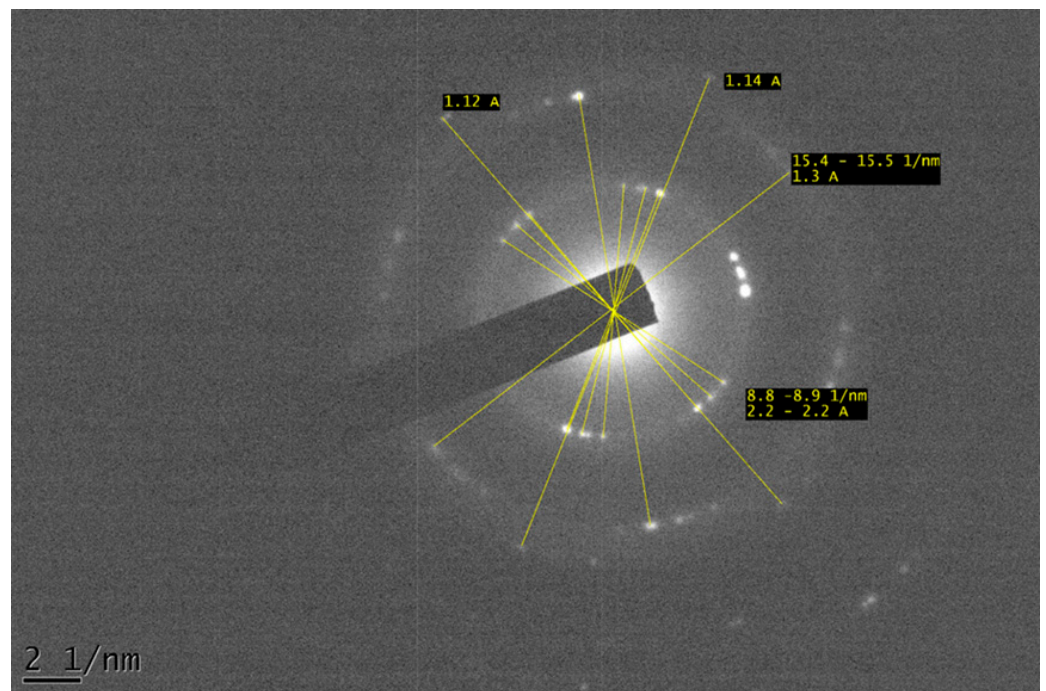
**Figure 3.** Selected area electron diffraction (SAED) on a graphene particle.

On the enlargement presented in Figure 4, several nanoparticles of copper oxide are seen aggregated and above the carbon surface, probably of a 3D particle of graphite of important size (more than 25 layers). A distance between fringes of 1.195 Å can be measured. This distance is confirmed by a Fourier mathematical transformation, and it is difficult to identify an inorganic species with one value only.
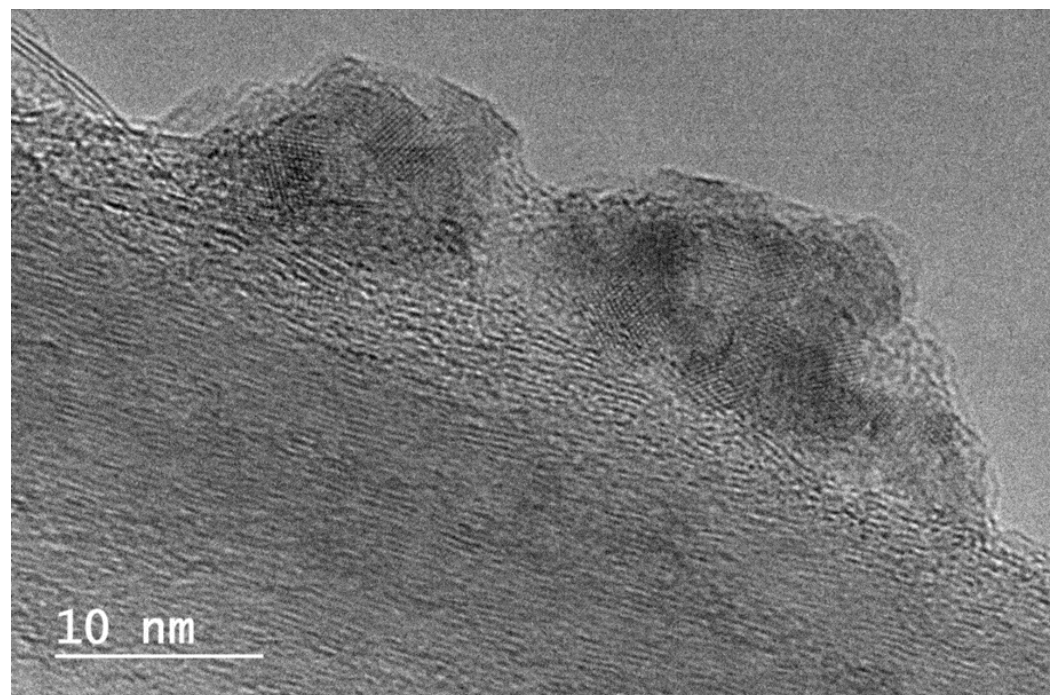


**Figure 4.** Details about copper oxide nanoparticles, external and covered by carbon layers. FFT on external oxide particles ($\times$500,000; scale bar 10 nm).

The SEM and TEM images are important, as they evidence thin 2D graphene sheets (five layers in Figure 3) mixed with more thick ones and also with 3D graphite (Figure 4). The information about the copper species was difficult to analyze since dehydration was used. The dried powder was deposited on a carbon grid covered by a carbon film. The sample was then left to dry for a long time before being introduced inside the TEM apparatus.

### 3.2.2. UV–Visible–NIR Spectroscopy
Before Copper Introduction

The measured absorbance was used to estimate the concentration of graphene sheets in suspension. We used the Beer–Lambert relation, $A = \varepsilon\, c\, l$, and a cell with an optical path of $l = 1$ cm. The absorbance, A, has no units. C is the graphene concentration and $\varepsilon$ the absorption coefficient in $L \cdot mol^{-1} \cdot cm^{-1}$.

Measurements were performed on two solutions, recovered after ultrasound treatments of 6 min. One solution is realized with pulses of 15 s for progressive dilutions in absolute ethanol and the other solution without. Four points corresponding to dilution by a factor of 0.10 to 0.35 were used, and the initial concentration of commercial graphite was 500 mg in 45 mL of absolute ethanol. Navik and Gai [23] have proposed for curcumin stabilized in water solutions of graphene that a preliminary value of ($\varepsilon\, c$) is 1650 mL/mg.

We present in Figure 5 the absorbance that can be measured after mixing several volumes, 1000, 750, and 500 µL, of the activated isolated solution immediately after ultrasound and centrifugation at 5000 rpm for 12 min with and without pulses. Dilution by absolute ethanol was carried out to obtain 4 mL of solution in each case (with 3 mL, 3.25 mL, and 3.5 mL, necessary to obtain an overall volume of 4 mL), and absorbance was measured on a quasi-flat straight line observed between 700 and 800 nm.
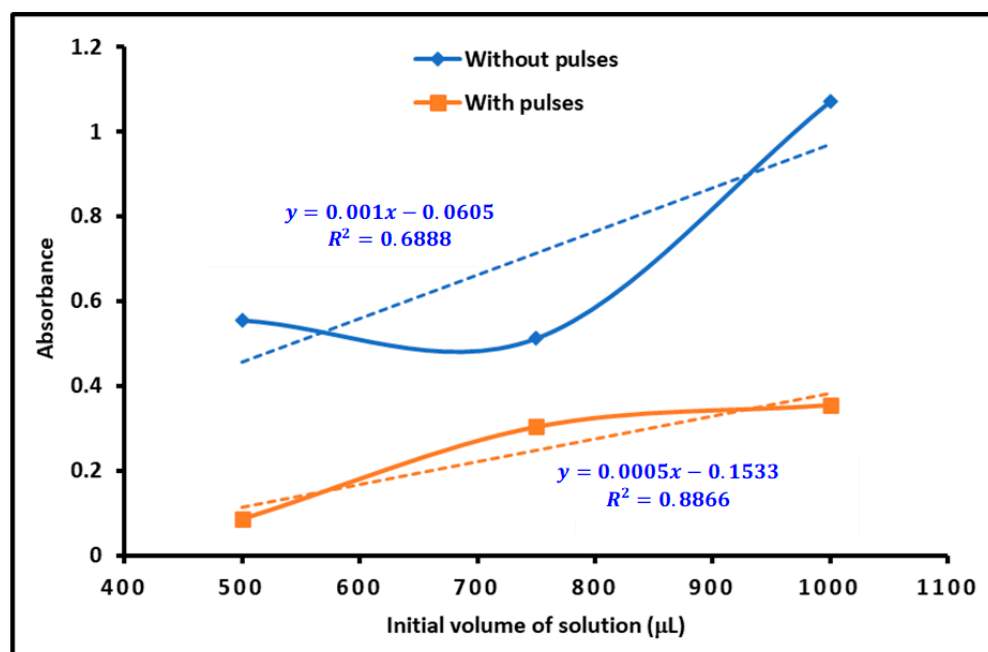


**Figure 5.** UV–visible results. Absorbance collected on dispersed graphene diluted in absolute ethanol: 1000, 750, and 500 µL diluted in 3.00, 3.25, and 3.50 mL of ethanol to obtain a total volume of 4 mL, studied in a 1 cm cell (in quartz) after ultrasound of 6 min, with and without pulses of 15 s and stops of 15 s, and centrifugation at 5000 rpm for 12 min.

Graphene was formed with pulses two more times. The corresponding overall weight of the C species in the solution was determined in an open Eppendorf tube and left to evaporate. No difference was measured with the two solutions made with 1000 and 750 µL with pulses: masses of 0.062 mg and 0.0605 mg of carbon were found. With the solution at

500 µL, the weight of carbon was equal to 0.0417 mg. Converted in µg by mL (with 4 mL total volume), this gives 15.5, 15.1, and 10.4 µg by ml of the diluted solution.

In practice, as detailed previously, dilution was necessary before collecting the UV–visible spectra. The necessary dilutions were performed taking an Eppendorf tube of 5 mL containing 250 µL of the selected "green" liquor, taken with a high-precision manual Eppendorf pipette BIOHT Proline 100–1000 µL, calibrated at 1% precision for 500 µL at room temperature (with a balance of precision of 0.001 g). The samples were dried in an autoclave at 60 °C for 2 h. The weight of the sample before and after drying was measured with a Mettler-Toledo scale (XPR204S maximum capacity 210 g, with a readability of 0.1 mg) after ethanol evaporation, and the final measured weight of the solid is due to the carbon contribution in the solution.

In Figure 6, a straight line is observed for the absorbance as a function of the detected C species in the flask containing the solution after ethanol evaporation. The linearity is better when the observed absorbance is plotted as a function of the concentration of carbon expressed in µg by ml. This line was used after to estimate the C amount in our ethanol solutions (without dilution). If we consider the point corresponding to 1000 µL of the solution prepared with 6 min of ultrasound and pulses of 15 s, it corresponds to 12.4 µg of C species by mL, and therefore there was 0.060 mg of suspended C species in the 5 mL of ethanol initially. Given the initial 500 mg of GR, this corresponds to a low percentage, less than 0.1% of the introduced C species. Compared with results published by Navik [22] that concern ultrasounds applied with a horn, a weight of C species in ethanol of 1.36 mg by ml, more than two times larger than ours, was obtained. The better obtained result was assigned to the use of large curcumin organic molecules that stabilize the graphene sheets. The power of the ultrasound treatment used was equal to 0.18, 0.54, 1.08, and 1.8 W in that publication, and we used about 40% of 500 W, which is more than 20 times more power but at 40% only. Despite the higher power that we used, our graphene suspension in ethanol was lower. More than the ultrasound power, this difference can be then assigned, according to Wallace and Shao [22], to the following parameters:

(1) The curcumin;
(2) The initial 3D graphite used;
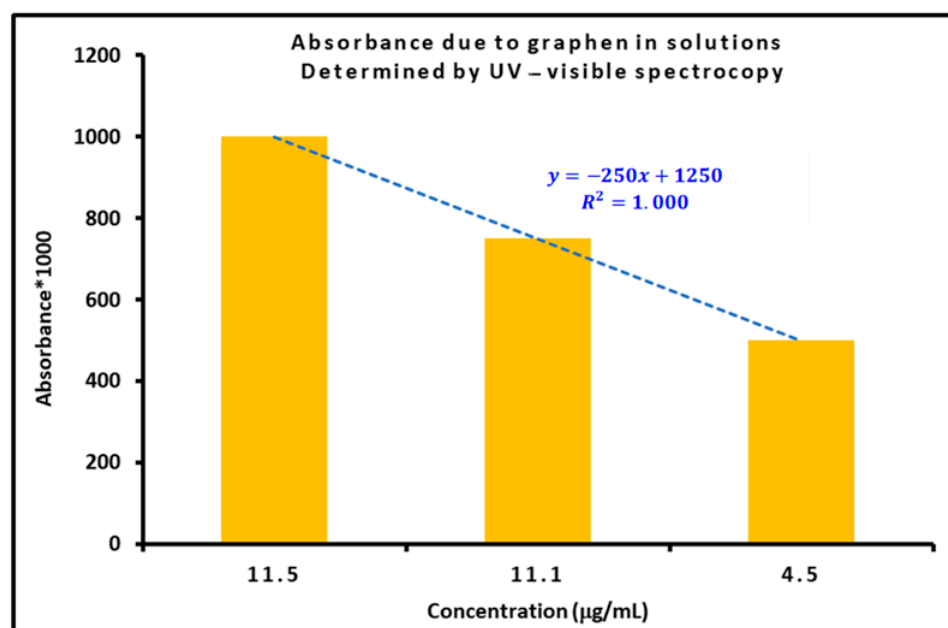(3) The duration of the ultrasound treatment applied (equal to 4 h).



**Figure 6.** Absorbance measured as a function of the composition of the studied solution expressed in µg by mL.

A weight of 50 mg by mL was obtained by Wallace and Shao [22], and this concentration is equal to 500 mg in 45 mL for a duration time equal to 6 min in our work.

Our calculations showed an average absorption coefficient equal to 2500 $L \cdot g^{-1} \cdot m^{-1}$, which is very close to that obtained by Hernandez et al. [26], with an absorption coefficient equal to 2240 $L \cdot g^{-1} \cdot m^{-1}$. The difference between the two results does not exceed 10%.

After Copper Chloride Addition

After centrifugation at 3000 rpm for 12 min, the solution was recovered and the solid $CuCl_2 \cdot 2H_2O$ salt was added; then, the salt was fully dissolved in less than 2 min, and the liquor exhibited a "green" homogeneous color. This treatment was reproduced with centrifugation at 5000 rpm 12 min. Possible ligands around the Cu(II) cations, in our conditions, are chloride anions, water, and ethanol molecules. The possible exchange of water molecules by ethanol from the solvent has been studied by Larin et al. [35]. In this study, it was also indicated that links with chloride anions were implying strongly acidic HCl solutions. We = then neglected chloride ligands, and concluded that we are dealing with $[Cu(H_2O)_{6-n} (Ethanol)_n$ with n < 3 complexes.

Figure 6 regroups the UV–visible spectra recorded with several graphene dispersions after the addition of $CuCl_2 \cdot 2H_2O$. Three distinct kinds of vibrations are observed: (1) in the UV range, vibrations of the C-C, C=C bonds of graphene and graphite; (2) still in the UV range between 300 and 400 nm, very intense vibrations due to collective excitation, in addition to plasmons of intensities greater than 10; (3) above 800 nm, broad vibrations of octahedral Cu(II) complexes (octahedral and tetrahedral).

On the right part of the visible spectrum, recorded with our more concentrated solution (Figure 6), are two broad peaks, one at 866 nm and a second one at 930 nm. It was observed that there was an exchange of ligands from water to ethanol, as detailed in Figure S2. Two distorted octahedral Cu(II) complexes are observed and assigned to trans and cis complexes of Cu(II), containing two ethanol and four water molecules. These species correspond to an axially distorted octahedral field in the visible spectrum that gives an averaged maximum at 866 nm. There is also a broad absorption observed at 930 nm on the spectrum of the most concentrated solution (Figures 7 and 8). Because of its position, this signal is attributed to Cu(I) species, possibly grafted on the graphene surface. They are stable in oxidation by oxygen molecules. Some protection by the solvent is necessary to explain their stability. Similar kinds of Cu species, grafted on C vacancies of carbon species on solid carbon diamonds, have been evidenced very recently [18]. They were investigated by demanding and expensive methods, EXAFS-XANES XANES [19], but also by less expensive operando IR measurements [18]. Here, we selected to use UV–visible–NIR spectroscopy.

Furthermore, on the left side of the spectrum, still with a concentrated solution, multiple and very intense peaks were detected between 309 and 371 nm (4.01 to 3.81 eV) with a second non-resolved broad peak between 262 and 371 nm. With progressive dilution, the narrow and intense peaks were eliminated, and the first peak was decomposed into at least three peaks, one at 230 nm and two above 250 nm. Further dilution shifted the broad peak to 265 nm, a position indicative of thin reduced graphene and attributed to the π-π* electronic transition, confirming the absence of graphene oxide (GO) in our diluted samples. For oxidized samples, a peak near 230 nm was reported. The intense additional peaks were attributed to plasmons associated with light reflection by graphene suspended nanoparticles. We observed that a simple dilution can eliminate their very intense peaks. A very similar result was obtained by changing the thickness of the used cell, going from 1 cm to an overall path of 2 mm internal (and 4 mm external). As illustrated in Figure 7, the intense reflections of plasmons are eliminated.
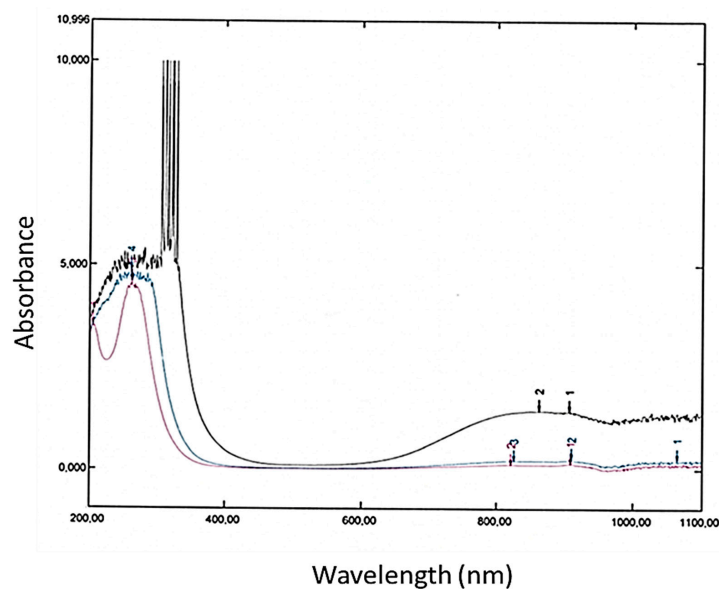
**Figure 7.** Influence of dilution by ethanol on UV–visible spectra of "green" liquors of Cu/graphene/ethanol. In black, preparation with 0.269 g commercial graphite: 45 mL absolute ethanol; ultrasound 7 min, and pulses of 15 s (in blue). Dilution "1": inside the UV cell, few drops inside 4 mL of absolute ethanol (in pink). Dilution "2": 1 mL of dilution "1" diluted with 3 mL ethanol (inside the visible cell).
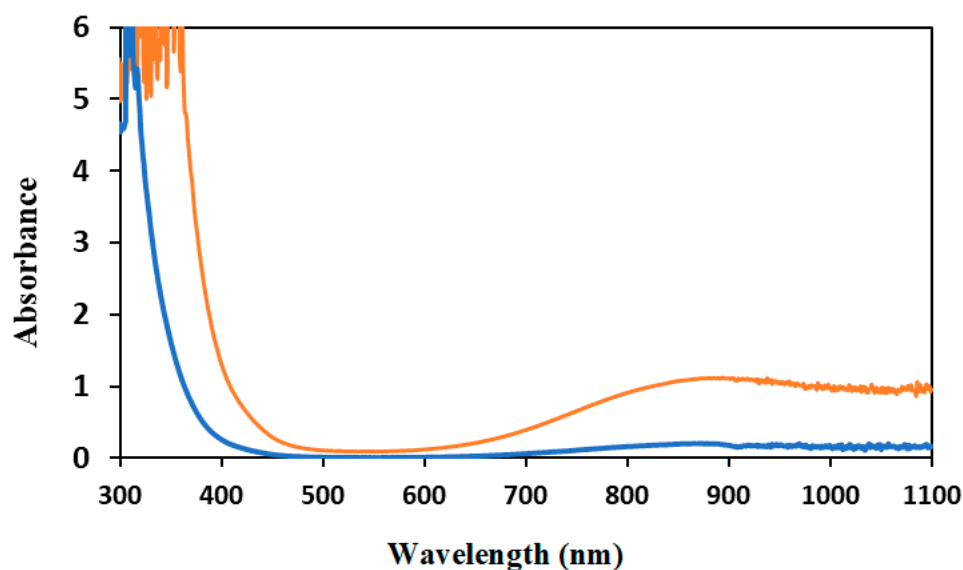


**Figure 8.** Influence of the optical path of UV–visible cells on plasmons coupling with the other vibrations: C-C vibrations on the left (from above to below 400 nm) and $[Cu\ Ethanol_2(H_2O)_4]^{2+}$ complex (864 nm instead of 800 nm for the hexa–aqua complex); orange in a cell of 1 cm and blue in a cell of 0.2 cm (internal).

It is incorrect to claim that graphene has a non-zero band-gap when it is dispersed inside a solvent dispersion. A band-gap, a difference in energy between its valence and its conduction band, is observed just after the plasmons in the UV spectral range, and its value is calculated here at the intersection between the most vertical line observed when going from 365 to 400 nm and the Ox axis. The spectra indicated a shift from 3.09 to 3.39 eV in its conversion of energy (eV) if the plasmons' contribution is removed. In the orange spectrum, coupling between them and the vibrations of graphene, its natural C-C, C=C bond is evidenced (Figure 8). Coupling between the added copper species and the plasmons is

also demonstrated by the position of the broad peak due to the $[Cu(H_2O)_6]^{2+}$ complex, which is shifting from above 850 nm down to its usual value circa 800 nm for the hexa–aqua complex in water.

Reduced graphene is a semi-conductor, and its band-gap can be estimated after conversion of the Ox axis of the visible spectrum in energy ($E = (h\,c)/\lambda$, where $h$ is the Planck constant, $c$ is the celerity of light in vacuum, and $\lambda$ is the light wavelength expressed in eV; the value is then converted into Joule and into eV, which gives $1238/\lambda$), with graphene highly dilutable in ethanol solutions. To obtain a Tauc plot, $\alpha$, the absorption coefficient, is calculated, knowing it is equal to $(1/d)\ln(T)$, with d, the thickness of the sample, being 1 cm with our cell, and $T$, transmission, equal to 10-power, which is the absorbance. Alpha multiplied by the photons' energy ($E\,\alpha$) power 0.5 is plotted versus the energy in eV, and straight lines are obtained. The corresponding band-gap for an indirect semi-conductor is obtained by calculation of the intercept of the lines with the vertical axis divided by the slope. An indirect value of 3.67 eV is obtained for the sample fabricated with 6 min of ultrasound. A value of 4.02 eV is obtained with the sample submitted to 2 h of ultrasound. The indirect value can be compared with published values: 4.7 eV (for a free-standing sheet of graphene) and 7.0 eV (graphite 3D) for a band attributed to a $\pi$-$\pi$* interband transition, as proposed and calculated by Politano and Chiarello in 2014 [9].

For a given concentration, there is a small peak at 230 nm on Figure 7, observed only with the smallest thickness path cell. This peak is due to contamination by oxidized C species that can be OH, peroxide, or COOH groups. At the highest concentration, a superposition with a negative absorption is observed, and the negative peak is masking traces of oxidized species. When the negative peak is present, no information about the oxidized species is available. After the elimination of the strong plasmons, a maximum of absorption is only observed at 270 nm in Figure 7, and this can be attributed to the reduced graphene sheets, without coupling with the other vibrations. They are composed of C atoms hybridized with $sp^2$, forming closed domains, the sizes of which are clearly evidenced by the presented UV spectra.

Care is necessary before using this value. Indeed, in old publications, the graphene sheets were in general considered to have a zero band-gap. It is obviously not the case here since we are studying graphene sheets dispersed on a solvent. In ethanol and if plasmons are suppressed, we observe a very strong absorption in the UV spectrum, and the existence of a band-gap in energy will be then confirmed by fluorescence spectra, as investigated next. We emphasize the fact that the band-gap energy can be measured using the Tauc expression recommended for indirect semi-conductors. A value of 3.67 eV is obtained with the larger graphene particles obtained after 6 min of ultrasound (Figure 9). Small sheets obtained after 2 h of ultrasound give a larger energy value of 4.02 eV because of a smaller number of involved C atoms and a less efficient $\pi$ delocalization.

Comparisons with published values for the band-gap of reduced graphene sheets are possible: values at 3.90, 3.60, and 3.20 eV have been published for nanoparticles obtained by the reduction of GO [16], with the decreasing value associated with differences in thicknesses. We assume that our two values of 4.02 and 3.67 eV are significantly different and rather associated with the dimension of graphene, from micron-size to smaller than 100 nm in the MEB and TEM images.
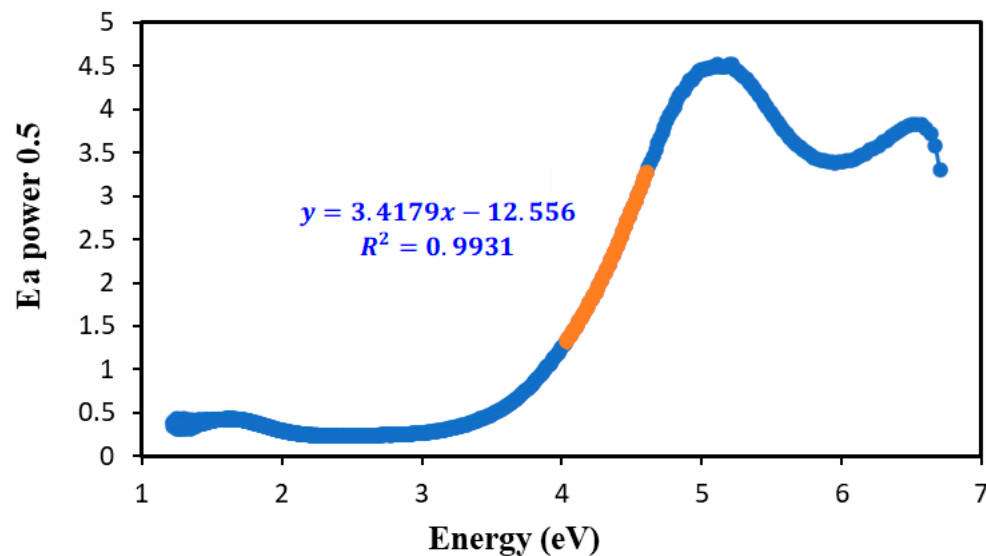
**Figure 9.** Associated TAUC plot for an indirect semi-conductor, obtained after 6 min of ultrasound treatment with pulses. The value of the band-gap is calculated by the extrapolation of the straight line in orange by dividing its origin (its common point with the Ox axis) by its slope. Here, a value of 3.67 eV is obtained.

### 3.2.3. Influence of Graphene Sizes Studied by Fluorescence (Emission) Spectra

The fluorescence of reduced graphene sheets was studied [30,31]. We tried two kinds of florescence measurements on our non-centrifugated liquors of graphene before the copper salt addition, the first one with ethanol and the second one directly with the concentrated initial black solutions, after a suspension of commercial graphite (GR) and ultrasound applied for 6 min and for 2 h. Better results were obtained without dilution and for an angle excitation light detector set at 90° to avoid detector saturation. The observed signals correspond to the superposition of signals attributed to graphite 3D and graphene 2D particles. The maximum shifts from 425 to 455 nm as the particle size increases from micron sizes to less than 100 nm in SEM and TEM images, involving fewer C atoms and lower energy $\pi$ delocalization.

The fluorescence spectrum of reduced rGO dissolved in water, acetone, ethyl acetate, toluene, and benzene with an excitation pulse of 300 nm is already published [30,31]. It was demonstrated that the fluorescence indeed exists and that the fluorescence properties were strongly affected by the solvent polarity.

Ethanol's polarity is larger than acetone's, and a free OH group also offers the possibility of H-bonds; therefore, we were expecting to observe a fluorescence signal in ethanol, as suggested by negative peaks seen in the UV spectra.

The detected fluorescence signals are presented in Figure 10 (Figure 10a ethanol only and Figure 10b with 2 h of the ultrasound treatment without applied centrifugation), with two spectra recorded on the small particles of graphite 3D and graphene 2D obtained by a 2 h ultrasound treatment and with an ultrasound treatment of 6 min. The two measurements were performed with the same energy of excitation (358 nm), the same rate (1 nm/s), and the same slit widths (external 5 nm, internal 2 nm).

The signal keeps a detectible intensity between 400 and 625 nm. The fluorescence spectra of rGO dissolved in water, benzene, toluene, ethyl acetate, and acetone at the excitation pulse of 300 nm have already been reported. The signal detected here in ethanol is stronger with the larger graphene nanoparticles obtained with 6 min of ultrasound treatment than after 2 h of ultrasound treatment. Its maximum shifts from 425 to 455 nm if the graphene particle size increases from micron sizes to lower than 100 nm in SEM and TEM images with fewer involved C atoms and a lower energy $\pi$ delocalization. The two measurements were performed with the same excitation of 358 nm, the same rate of 1 nm by s, and the same slit widths, external of 5 nm and internal of 2 nm.
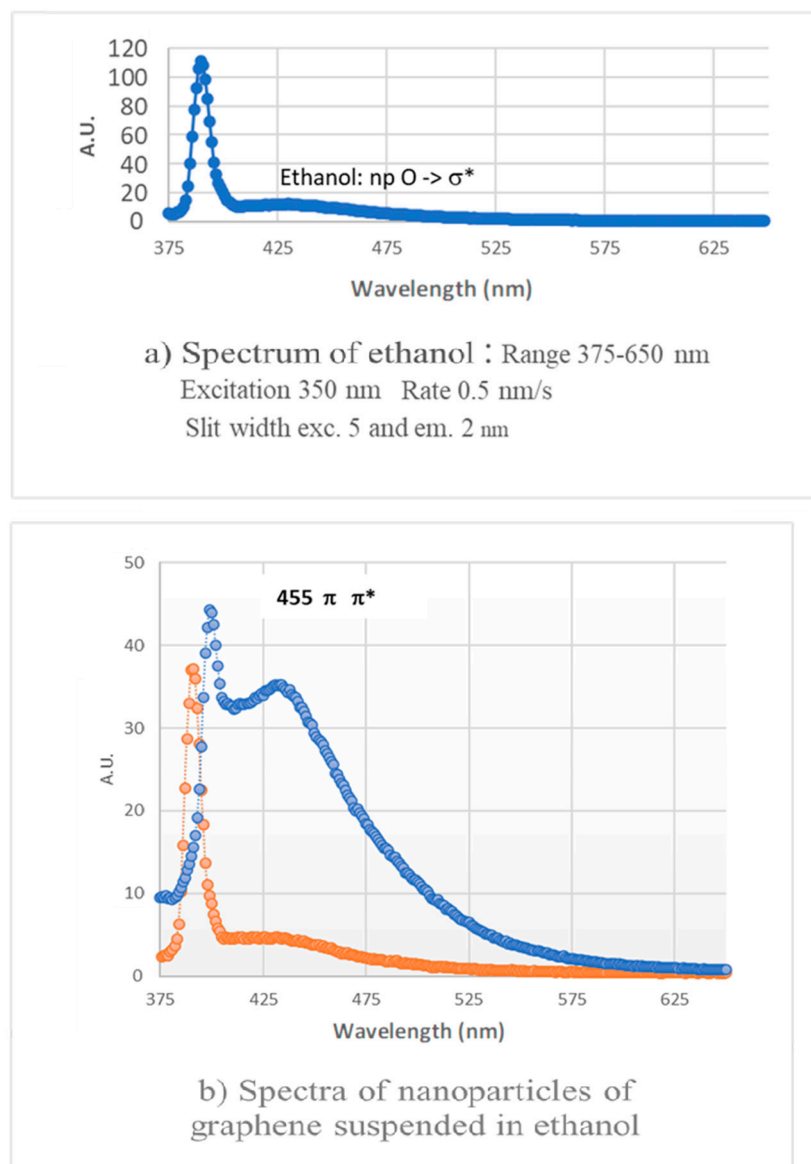
**Figure 10.** Fluorescence spectra of ethanol of two solutions of graphite 3D and graphene 2D suspended in ethanol prepared with 6 min (**a**) and with 2 h of the ultrasound treatment, respectively (excitation at 358 nm), without applied centrifugation (**b**). The existence of the 2D particles is demonstrated by SAXS measurements presented in the Supplementary Information—comparison of the SAXS results obtained on the powder after centrifugation and of the powder recovered by filtration on the solution on paper and drying in air.

3.2.4. Reactivity Test

UV–visible spectra were necessary to follow the oxidation of two organic dyes (eosin and bromophenol blue). With eosin, the initial concentration of the dye was equal to 44 mg in 100 mL of distilled water, while the blue bromophenol dye was in water. Dilutions were then prepared and were necessary to collect UV–visible–NIR spectra:

(1) An amount of 250 µL of the initial solution was diluted in 4 mL of distilled water, directly inside a 1 cm cell in quartz;

(2) Dilution 2 was prepared by the dilution of 250 µL of dilution 1 into 4 mL of distilled water;

(3) Dilution 3 was prepared with 250 µL of dilution 2 into 4 mL of water. To these dilutions, 250 µL of liquid was removed and replaced with 250 µL of the active liquor.

With the three solutions, the characteristic peaks of the eosin dye were located at 503 and 534 nm, with relative absorbances of 0.503 and 1.15 for dilution 3. The three peaks were eliminated in seconds with a few drops of the active green liquors that we tested both with small and with large rGO particles. A similar treatment was undertaken with a blue bromophenol dye in water. The treatments were also reproduced in ethanol.

It is important to know that no plasmons of rGO were present in the used dilutions. This was on purpose to study the material's photocatalytic activity in their absence.

## 4. Conclusions and Perspectives

Ultrasound treatments of ethanol dispersions of a commercial graphite (GR) were very efficient to obtain reduced and "flat" graphene sheets that we characterized by XRD, SEM, and TEM. UV–visible–NIR results were complemented by fluorescence spectroscopy. For ultrasound treatments at a power of 500 W (used at 40% and with a frequency of 20 MHz), a horn was directly introduced inside the solution, and the treatments were performed either with a constant method or using pulses of 15 s and stops of 15 s for overall times of 5–7 min and of 2 h.

Thanks to the systematic use of centrifugation vials having the same volume (45 mL) of solvent, the same amount of commercial C-based GR species, and similar centrifugation conditions, we can conclude that the graphene sheet dimension was directly affected by the time of the ultrasound treatment used. The main dimension of the graphene particles decreased from larger than a micron (ultrasound of 6 min) to smaller than 100 nm (after ultrasound of 2 h). Even after 2 h of ultrasound treatment, the C particles remained stacked, and more than 5 to 25 sheets were detected.

Interesting plasmons (collective excitation of electrons, considered as a gaseous plasma) were observed after centrifugation and the addition of $CuCl_2 \cdot 3H_2O$, and both their intensities (absorption that can be larger than 10) and their positions were affected by dilutions. The existence of a coupling between the plasmons and the vibrations of the C lattice was demonstrated. At a high dilution to remove the plasmons, the prepared Cl/Cu/graphene solutions were very strong oxidants, as demonstrated by catalytic tests performed with a dye (eosin and bromophenol blue in water and in ethanol). In our experimental conditions, the visible signal of the dye was indeed eliminated in a few seconds with both small and large rGO particles.

In the future, more concentrated solutions will be used to preserve plasmons. A more complete study including several solvents of varied polarity and using atomic force microscopy will be in progress. In addition, we will study the molecular interactions between copper, rGO, and added organic molecules, and we will propose a dynamic process.

**Data Availability Statement:** There are no additional data. The original contributions presented in the study are included in the article.

**Conflicts of Interest:** The authors declare no conflicts of interest.

## References

1. Fuchs, J.N.; Goerbig, M.O. Le graphène premier crystal bidimensionnel. *Pour La Sci. Phys.* **2008**, *367*, 36–43.
2. Mbayachi, B.; Ndayiragije, E.; Sammani, T.; Taj, S.; Mbuta, E.R.; Khan, A.U. Graphene synthesis, characterization and its applications: A review. *Results Chem.* **2021**, *3*, 100163. [CrossRef]
3. Li, X.; Yu, J.; Wageh, S.; Al-Ghamdi, A.A.; Xie, J. Graphene in Photocatalysis: A Review. *Small* **2016**, *12*, 6640–6696. [CrossRef]
4. Minzhen, C.; Thorpe, D.; Adamson, D.H.; Schniepp, H.C. Methods of Graphite Exfoliation. *J. Mater. Chem.* **2012**, *22*, 24992. [CrossRef]
5. Ikram, M.; Sarfraz, A.; Aqeel, M.; Ul-Hamid, A.; Imran, M.; Haider, J.; Haider, A.; Shahbaz, A.; Salamat, A. Visible-Light-Induced Dye Degradation over Copper-Modified Reduced Graphene Oxide. *J. Alloys Compd.* **2020**, *837*, 155588. [CrossRef]
6. Grasseschi, D.; Silva, W.C.; de Souza Paiva, R.; Starke, L.D.; do Nascimento, A.S. Surface coordination chemistry of graphene: Understanding the coordination of single transition metal atoms. *Coord. Chem. Rev.* **2020**, *422*, 21346. [CrossRef]
7. Huang, F.; Deng, Y.; Chen, Y.; Cai, X.; Peng, M.; Jia, Z.; Xie, J.; Xiao, D.; Wen, X.; Wang, N.; et al. Anchoring $Cu_1$ species over nanodiamond-graphene for semi-hydrogenation of acetylene. *Nat. Commun.* **2019**, *10*, 4431. [CrossRef]
8. Zhang, L.; Yang, X.; Yuan, Q.; Wei, Z.; Ding, J.; Chu, T.; Rong, C.; Zhang, Q.; Ye, Z.; Xuan, F.Z.; et al. Elucidating the structure-stability relationship of Cu single-atom catalysts using *operando* surface-enhanced infrared absorption spectroscopy. *Nat. Commun.* **2023**, *14*, 8311. [CrossRef]
9. Li, L.; Li, M.; Zhang, R.; Zhang, Q.; Geng, D. Liquid Cu–Zn catalyzed growth of graphene single-crystals. *New J. Chem.* **2023**, *47*, 20703–20707. [CrossRef]
10. Tabaja, N.; Brouri, D.; Casale, S.; Zein, S.; Jaafar, M.; Selmane, M.; Toufaily, J.; Davidson, A. Use of SBA-15 silica Grains for Engineering Mixtures of Co Fe and Zn Fe SBA-15 for Advanced Oxidation Reactions under UV and NIR. *Appl. Catal. B Environ.* **2019**, *253*, 369–378. [CrossRef]
11. Chettah, W.; Barama, S.; Medjram, M.-S.; Selmane, M.; Montero, D.; Davidson, A.; Védrine, J.C. Anatase titania activated by Cu(II) or Zn(II) nanoparticles for the photooxidation of methanol assisted by Rhodamine-B. *Mater. Chem. Phys.* **2021**, *257*, 123714. [CrossRef]
12. Ghazinejad, M.; Hosseini Bay, H.; Reiber Kyle, J.; Ozkan, M. Fluorescence quenching metrology of graphene. *SPIE Proc.* **2014**, *8994*, 169–175.
13. Jubu, P.R.; Yam, F.K.; Igba, V.M.; Beh, K.P. Tauc-plot scale and extrapolation effect on bandgap estimation from UV–vis–NIR data—A case study of β-$Ga_2O_3$. *J. Solid State Chem.* **2020**, *290*, 121576. [CrossRef]
14. Tabaja, N. Nanoparticules d'oxydes de fer et de Ferrites Obtenues par Nano-Réplication: Réactivité Chimique et Application en Dépollution des Eaux. Ph.D. Thesis, Université Pierre et Marie Curie-Paris VI, Paris, France, Université Libanaise, Beirut, Lebanon, 2015. Available online: https://theses.fr/070382972 (accessed on 10 May 2024).
15. Jezzini, A. $ZnFe_2O_4$ for Heterogeneous Photocatalysis in the Visible Spectrum. Ph.D. Thesis, Sorbonne Université, Paris, France, 2020.
16. Shenoy, R.U.K.; Rama, A.; Govindan, I.; Naha, A. The purview of doped nanoparticles: Insights into their biomedical applications. *OpenNano* **2022**, *8*, 100070. [CrossRef]
17. Larin, G.M.; Minin, V.V.; Levin, B.V.; Buslaev, Y.A. *Complexation in the $CuCl_2\_C_2H_5OH\_H_2O$ System*; N. S. Translated from Izvestiya Akademii Nauk SSSR, Seriya Khimicheskaya; Kurnakov Institute of General and Inorganic Chemistry, Academy of Sciences of the USSR: Moscow, Russia, 1990; Volume 12, pp. 2725–2729.
18. Mak, K.F.; Ju, L.; Wang, F.; THeinz, F. Optical spectroscopy of graphene: From the far infrared to the ultraviolet. *Solid Stat. Commun.* **2012**, *152*, 1341–1349. [CrossRef]
19. Kumar, P. Bandgap Measurement of Reduced Graphene Oxide Monolayers through Scanning Tunneling Spectroscopy. *arXiv* **2019**, arXiv:1911.06230.
20. Li, H.; Papadakis, R.; Hassan, S.; Jafri, M.; Thersleff, T.; Michler, J.; Ottosson, H.; Leifer, K. Superior adhesion of graphene nanoscrolls. *Common. Phys.* **2018**, *1*, 44. [CrossRef]
21. Atri, P.; Tiwari, D.C.; Sharma, R. Synthesis of reduced graphene oxide nanoscrolls embedded in polypyrrole matrix for supercapacitor applications. *Synth. Met.* **2017**, *227*, 21–28. [CrossRef]
22. Wallace, J.; Shao, L. Defect-induced carbon nanoscroll formation. *Carbon* **2015**, *91*, 96. [CrossRef]

23. Jezzini, A.; Chen, Y.; Davidson, A.; Hamieh, T.; Toufailly, J. Photocatalytic Decomposition of Amoxicillin Using Zinc Ferrite Nanoparticles. *Crystals* **2024**, *14*, 291. [CrossRef]

24. Faniyi, O.; Fasakin, O.; Olofinjana, B.A.; Adekunle, S.; Oluwasusi, T.V.; Eleruja, M.A.; Ajayi, E.O.B. The comparative analyses of reduced graphene oxide (rGO) prepared via green, mild and chemical approaches. *SN Appl. Sci.* **2019**, *1*, 1181. [CrossRef]

25. Thiurnina, A.V. Ultrasonic exfoliation of graphene in water: A key parameter study. *Adv. Mater.* **2010**, *22*, 1039–1059. [CrossRef]

26. Navik, R.; Gai, Y.; Wang, W.; Zhao, Y. Curcumin-assisted ultrasound exfoliation of graphite to graphene in ethanol. *Ultrason. Sonochem.* **2018**, *48*, 96–102. [CrossRef]

27. Muthosamy, K.; Manickam, S. State of the art and recent advances in the ultrasound-assisted synthesis, exfoliation and functionalization of graphene derivatives. *Ultrason. Sonochem.* **2017**, *39*, 478–493. [CrossRef]

28. Simani, M.; Dehghani, H. The study of electrochemical hydrogen storage behavior of the UiO-66 framework on the metal/reduced graphene oxide substrate. *Fuel* **2023**, *341*, 127624. [CrossRef]

29. Kuterasiński, L.; Podobiński, J.; Madej, E.; Smoliło-Utrata, M.; Rutkowska-Zbik, D.; Datka, J. Reduction and Oxidation of Cu Species in Cu-Faujasites has been Studied by IR Spectroscopy. *Molecules* **2020**, *25*, 4765. [CrossRef]

30. Rosa Axet, M.; Durand, J.; Gouygou, M.; Serp, P. Surface coordination chemistry on graphene and two-dimensional carbon materials for well-defined single atom supported catalysts. *Adv. Organomet. Chem.* **2019**, *71*, 53–73. [CrossRef]

31. Yao, D.; Wang, Y.; Li, Y.; Li, A.; Zhen, Z.; Lv, J.; Sun, F.; Yang, R.; Luo, J.; Jiang, Z.; et al. Scalable synthesis of Cu clusters for remarkable selectivity control of intermediates in consecutive hydrogenation. *Nat. Commun.* **2023**, *14*, 1123. [CrossRef] [PubMed]

32. Zhao, Y.; Tao, L. Towards catalytic reactions of Cu single-atom catalysts: Recent progress and future perspective. *Chin. Chem. Lett.* **2024**, *35*, 108571. [CrossRef]

33. Bhaumik, A.; Narayan, J. Reduced Graphene Oxide-Nanostructured Silicon Photosensors with High Photoresponsivity at Room Temperature. *ACS Appl. Nano Mater.* **2019**, *2*, 2086–2098. [CrossRef]

34. Politano, A.; Chiarello, G. Plasmon modes in graphene: Status and prospect. *Nanoscale* **2014**, *6*, 10927–10940. [CrossRef] [PubMed]

35. Drosou, M.; Mitsopoulou, C.A.; Orio, M.; Pantazis, D.A. EPR Spectroscopy of Cu(II) Complexes: Prediction of *g*-Tensors Using Double-Hybrid Density Functional Theory. *Magnetochemistry* **2022**, *8*, 36. [CrossRef]